Geophysical Research Letters

Supporting Information for

Sediment oxygen uptake and hypoxia: a simple mass-balance model for estuaries and coastal oceans

Jing Sun[1,2], Liuqian Yu[2,3*], Xingyu Yang[1,2], Jianping Gan[1,2], Hongbin Yin[4], and Jiying Li[1,2*]

[1]Department of Ocean Science, The Hong Kong University of Science and Technology, Clear Water Bay, Kowloon, Hong Kong SAC, P. R. China

[2]Center for Ocean Research in Hong Kong and Macau, Hong Kong SAC, P. R. China

[3]Earth, Ocean and Atmospheric Sciences Thrust, The Hong Kong University of Science and Technology (Guangzhou), Guangdong, P.R. China

[4]Nanjing Institute of Geography and Limnology, Chinese Academy of Science, Nanjing, Jiangsu, P. R. China

Contents of this file

Introduction

The supporting information (SI) includes a detailed description of the methods (S1), the mass balance model (S2), and how the data is used to obtain the fitted parameter spatial reactivity (S3). The SI also includes a table summarizing the physicochemical properties of all sites (Table S1), a table listing all the parameters used in the model and their descriptions (Table S2), a table including data from other coastal systems (Table S3), and eight figures (Figs. S1-S8) supporting the discussion in the main text.

S1. Methods

Samples were collected during the summer of 2021 from the Pearl River Estuary and its adjacent continental shelf waters (PRE region) (Li et al. 2024). We used a Sea-Bird SBE17 plus conductivity–temperature–depth (CTD) probe to measure the temperature, density, salinity, and dissolved O_2 concentrations. Chlorophyll (Chl-a) fluorescence obtained from the CTD probe was calibrated by measuring Chl-a fluorometrically (APHA, 1998) in the water samples taken from various depths by using Niksin bottles attached on the CTD. We calculate the buoyancy frequency (N^2 (s^{-2})) to indicate the stratification of the water column:

$$N^2 = \frac{g}{\rho(z)}\frac{d\rho(z)}{dz} \quad \text{Eq. S1}$$

where g is the gravity acceleration (9.80665 m s^{-2}), z is the water depth (m) with zero at the sea surface and positive downwards; ρ is the potential density (kg m^{-3}) calculated using the Gibbs-SeaWater Oceanographic Toolbox (GSWOT) and data obtained by the CTD probes, including temperature, salinity, depth, pressure, and geographic coordinates (McDougall & Barker, 2011). Higher N^2 implies high stability of the water column.

Sediment cores were collected with undisturbed overlying waters of around 15-20 cm using a Uwitec corer (core liners of 86 mm ID and 60 cm length). The sediment's oxygen micro-profiles (of 0.5-1 mm resolution) were obtained using a micro-profiling system equipped with a Unisense O_2 electrode, calibrated using the air-saturated seawater and zero oxygen solution at in-situ temperature. The sediment-water interface was defined as the depth where the sharpest oxygen gradient was observed, which was consistent with our visual observation of the interface. Oxygen penetration depth (OPD) was defined as the depth where the oxygen concentration under the detection limit of ~ 0.3 μmol L^{-1}. The sediment physical properties, including water content and densities, were quantified and reported in (Zhou, 2022).

The total sediment oxygen uptake (SOU) was determined using whole-core incubations: sediment cores were stabilized, and the overlying water was gently bubbled with air to compensate for the oxygen lost between sample collection and incubation. The sediment cores were then tightly sealed with rubber stoppers to start the incubation, during which the overlying waters were gently stirred with a stir bar located at ~ 5 cm above the sediment-water interface to generate the movement of overlying water and create a diffusive boundary layer (Jørgensen & Revsbech, 1985). The cores were covered with aluminum foil to avoid the potential disturbance from light, and the oxygen concentration in the overlying water was monitored using an oxygen optical probe (Pyroscience). The incubation typically lasts around 2-3 hours, during which ~ 20% dissolved oxygen in the overlying water was consumed. The SOU (mmol O_2 m^{-2} d^{-1}) was obtained from the linear decrease of oxygen in the overlying waters. Onboard measurements were conducted within 2-6 hours after sampling.

S2. The mass balance model for oxygen

The paper focuses on oxygen budget in the bottom waters (or BBL). For clarity, we will first introduce the mass balance model for the entire water column, followed by the model in the BBL that can be understood using similar logic.

S2.1 The oxygen mass balance

The O_2 budget of the entire water column can be written as changes in oxygen concentrations contributed by fluxes from the atmosphere, sediments, and net consumption within the water column:

$$\frac{\mathrm{d}\bar{C}_{\mathrm{w-O2}}}{\mathrm{d}t} = \frac{F_{\mathrm{AWI-O2}}}{H} - \frac{F_{\mathrm{SWI-O2}}}{H} + \frac{\int_0^H R_{\mathrm{w-O2}}\,\mathrm{d}z_{\mathrm{w}}}{H} \qquad \text{Eq. S2}$$

Here, $\bar{C}_{\mathrm{w\text{-}O2}}$ is the oxygen concentration ($C_{\mathrm{w\text{-}O2}}$) integrated over the entire water column divided by the total depth of the water column (H): $\bar{C}_{\mathrm{w-O2}} = (\int_0^H C_{\mathrm{w-O2}}\,\mathrm{d}z_{\mathrm{w}})/H$, which is also the average O_2 concentration in the water column. $F_{\mathrm{AWI\text{-}O2}}$ and $F_{\mathrm{SWI\text{-}O2}}$ are the O_2 fluxes at the air-water interface (AWI) and sediment-water interface (SWI), respectively (positive means downward flux, thus $F_{\mathrm{AWI\text{-}O2}}$ describes oxygen entering the water column and $F_{\mathrm{SWI\text{-}O2}}$ describes oxygen leaving the water column); $R_{\mathrm{w\text{-}O2}}$ is the rate of oxygen in the water column (negative means consumption); z_{w} is the downward vertical displacement in the water column reference to the air-sea interface (positive indicates going downwards). All parameters are described in Table S2.

The integration of the O_2 rate over the entire water column can be defined as the O_2 reaction flux in the water column ($F_{\mathrm{w\text{-}O2}}$):

$$\int_0^H R_{\mathrm{w-O2}}\,\mathrm{d}z_{\mathrm{w}} = F_{\mathrm{w-O2}} \qquad \text{Eq. S3}$$

Here, negative $F_{\mathrm{w\text{-}O2}}$ means oxygen consumption in the water column. Similarly, integrating the O_2 rate in the sediments ($R_{\mathrm{s\text{-}O2}}$) can be defined as the O_2 reaction flux in the sediment ($F_{\mathrm{s\text{-}O2}}$):

$$\int_0^{+\infty} R_{\mathrm{s-O2}}\,\mathrm{d}z_{\mathrm{s}} = F_{\mathrm{s-O2}} \qquad \text{Eq. S4}$$

Here, z_{s} is the vertical displacement in the sediment column (z_{s} =0 at the sediment-water interface, and positive indicates going downwards) and negative $F_{\mathrm{s\text{-}O2}}$ means oxygen consumption in the sediments. The sediment oxygen consumption (negative $F_{\mathrm{s\text{-}O2}}$) is equivalent to downward fluxes (positive $F_{\mathrm{SWI\text{-}O2}}$):

$$F_{\mathrm{s-O2}} = -F_{\mathrm{SWI-O2}} \qquad \text{Eq. S5}$$

This can also be understood by considering the mass balance of O_2 for the entire sediment column, as total oxygen consumption ($F_{\mathrm{s\text{-}O2}}$) should cancel out the amount of oxygen coming into the sediment from the water column ($F_{\mathrm{SWI\text{-}O2}}$): $F_{\mathrm{s\text{-}O2}} + F_{\mathrm{SWI\text{-}O2}} = 0$. Combing Eqs. S2-5 yields:

$$\frac{\mathrm{d}\bar{C}_{\mathrm{w-O2}}}{\mathrm{d}t} = \frac{F_{\mathrm{AWI-O2}}}{H} + \frac{F_{\mathrm{s-O2}}}{H} + \frac{F_{\mathrm{w-O2}}}{H} \qquad \text{Eq. S6}$$

S2.2 Oxygen consumption and flux in the sediment

The fluxes (integrated rates) of oxygen ($F_{\mathrm{w\text{-}O2}}$ and $F_{\mathrm{s\text{-}O2}}$) can be approximated as the integrated rates of carbon mineralization for water and sediment columns, respectively, assuming oxygen in the water and sediments is mostly consumed by remineralization of organic matter and its reduced products and a close to 1:1 ratio between organic carbon

remineralization and oxygen consumption. The reaction rates of O_2 in sediments ($R_{s\text{-}O2}$) can then be described using a first-order kinetic model:

$$R_{\mathrm{s-O2}} = \frac{\mathrm{d}C_{\mathrm{s-C}}}{\mathrm{d}t} = -k_{\mathrm{s}} C_{\mathrm{s-C}} \qquad \text{Eq.S7}$$

Here, $C_{s\text{-}C}$ and k_s are the concentration and reactivity of organic carbon in the sediment, respectively. The solution of Eq.S7 is

$$C_{\mathrm{s-C}} = C^0_{\mathrm{s-C}} e^{-k_{\mathrm{s}} t} \qquad \text{Eq.S8}$$

where $C^0_{\mathrm{s-C}}$ is organic carbon concentration at the sediment-water interface; t is the age of the sediment layer reference to its initial deposition on the seafloor, which is also the time for sediment to be buried from the sediment surface to its current depth (z_s) with a sediment burial velocity of u_s. Therefore,

$$t = \frac{z_{\mathrm{s}}}{u_{\mathrm{s}}} \qquad \text{Eq.S9}$$

and Eq.S8 becomes

$$C_{\mathrm{s-C}} = C^0_{\mathrm{s-C}} e^{-k_{\mathrm{s}} (\frac{z_{\mathrm{s}}}{u_{\mathrm{s}}})} = C^0_{\mathrm{s-C}} e^{-(\frac{k_{\mathrm{s}}}{u_{\mathrm{s}}}) z_{\mathrm{s}}} \qquad \text{Eq. S10}$$

Combining Eqs. S4, 5, and 10,

$$F_{\mathrm{s-O2}} = \int_0^{+\infty} R_{\mathrm{s-O2}}\, \mathrm{d}z_{\mathrm{s}} = -\int_0^{+\infty} k_{\mathrm{s}}\, C^0_{\mathrm{s-C}}\, e^{-\left(\frac{k_{\mathrm{s}}}{u_{\mathrm{s}}}\right) z_{\mathrm{s}}}\, \mathrm{d}z_{\mathrm{s}} = -\, C^0_{\mathrm{s-C}}\, u_{\mathrm{s}} \qquad \text{Eq. S11}$$

Intuitively, oxygen is consumed due to the downward flux of organic carbon into the sediments ($C^0_{\mathrm{s-C}}\, u_{\mathrm{s}}$), which is also the flux from the water column ($C^H_{\mathrm{w-C}}\, u_{\mathrm{w}}$) considering the mass balance:

$$F_{\mathrm{s-O2}} = -\, C^0_{\mathrm{s-C}}\, u_{\mathrm{s}} = -\, C^{\mathrm{H}}_{\mathrm{w-C}}\, u_{\mathrm{w}} \qquad \text{Eq. S12}$$

Here, $C^H_{\mathrm{w-C}}$ is the organic carbon concentration in the water column at the seafloor (z_w=H) and u_{w} is the particle settling velocity in the water column. However, Eqs. S11 and S12 assume a constant reactivity of the organic matter in the sediments (k_s), and all the organic carbon can be eventually decomposed. In reality, reactivity should decrease as the organic matter becomes older (Li et al., 2012; Middelburg, 1989), and at a certain depth, the organic matter would be too old and refractory (k_s becomes too small). For simplicity, Eqs. S11 and S12 can be corrected using an efficiency (ε) of organic carbon remineralization in the sediments:

$$F_{\mathrm{s-O2}} = -\varepsilon C^0_{\mathrm{s-C}} u_{\mathrm{s}} = -\varepsilon C^H_{\mathrm{w-C}}\, u_{\mathrm{w}} \qquad \text{Eq.S13}$$

S2.3 Oxygen consumption and flux in the water column

Similarly, in the water column, if we assume the decay of organic matter follows a first-order model as in the sediments:

$$R_{\mathrm{w-O2}} = \frac{\mathrm{d}C_{\mathrm{w-C}}}{\mathrm{d}t} = -k_{\mathrm{w}} C_{\mathrm{w-C}} \qquad \text{Eq.S14}$$

Here, $C_{w\text{-}C}$ and k_w are the concentration and reactivity of organic carbon in the water column, respectively. The concentration of organic carbon can then be described similarly to Eq. S10:

$$C_{\mathrm{w-C}} = C^0_{\mathrm{w-C}} e^{-k_{\mathrm{w}} (\frac{z_{\mathrm{w}}}{u_{\mathrm{w}}})} = C^0_{\mathrm{w-C}} e^{-(\frac{k_{\mathrm{w}}}{u_{\mathrm{w}}}) z_{\mathrm{w}}} \qquad \text{Eq.S15}$$

where $C^0_{\mathrm{w-C}}$ is the organic carbon concentration in the surface water (z_w=0). The concentration of organic matter on the seafloor ($C^H_{\mathrm{w-C}}$) is

$$C^H_{\mathrm{w-C}} = C^0_{\mathrm{w-C}} e^{-(\frac{k_w}{u_w})H} \quad \text{Eq.S16}$$

Therefore, combining Eqs.S3, S14, S15, and S16 yields the oxygen reaction flux in the water column:

$$F_{\mathrm{w-O2}} = \int_0^H -k_w C_{\mathrm{w-C}}\,\mathrm{d}z_w = \int_0^H -k_w C^0_{\mathrm{w-C}} e^{-k_w(\frac{z_w}{u_w})}\,\mathrm{d}z_w = C^0_{\mathrm{w-C}} u_w (e^{-(\frac{k_w}{u_w})H} - 1) \quad \text{Eq.S17}$$

Combining Eqs.S13 and 16 yields

$$F_{\mathrm{s-O2}} = -\varepsilon C^H_{\mathrm{w-C}}\, u_w = -\varepsilon C^0_{\mathrm{w-C}} e^{-(\frac{k_w}{u_w})H} u_w \quad \text{Eq.S18}$$

Therefore, from Eqs. S17 and S18, the oxygen flux in the water column and sediments has an intrinsic relationship:

$$F_{\mathrm{w-O2}} = \frac{1}{\varepsilon}(e^{(\frac{k_w}{u_w})H} - 1) F_{\mathrm{s-O2}} \quad \text{Eq.S19}$$

For simplicity, we introduce a rate parameter termed spatial reactivity (f, or spatial frequency) to characterize the reaction of oxygen in the water column, by normalizing the temporal frequency (temporal reactivity k_w, in the unit of d^{-1}) to the particles settling velocity (u_w):

$$f = \frac{k_w}{u_w} \quad \text{Eq. S20}$$

Similar to temporal reactivity (k_w) that refers to the reaction proceeded per unit of time (see Eq. S14), the spatial frequency (f; in unit of m^{-1}) describes the reaction proceeded per unit distance the particles settle downwards. In other words, Eq. S14 becomes

$$R_{\mathrm{w-O2}} = \frac{\mathrm{d}C_{\mathrm{w-C}}}{\mathrm{d}z_w} = -f C_{\mathrm{w-C}} \quad \text{Eq. S21}$$

Eq. S19 can then be simplified as

$$F_{\mathrm{w-O2}} = \frac{1}{\varepsilon}(e^{fH} - 1) F_{\mathrm{s-O2}} \quad \text{Eq. S22}$$

S2.4 Apparent oxygen utilization (AOU) in the water column

Now consider the water column experiencing oxygen loss from its equilibrium saturation concentration to the current state over a period of *T*. From Eq. S6,

$$\int_0^T \frac{\mathrm{d}\bar{C}_{\mathrm{w-O2}}}{\mathrm{d}t}\mathrm{d}t = \int_0^T \left(\frac{F_{\mathrm{AWI-O2}}}{H} + \frac{F_{\mathrm{s-O2}}}{H} + \frac{F_{\mathrm{w-O2}}}{H}\right)\mathrm{d}t \quad \text{Eq. S23}$$

Assuming the fluxes ($F_{\mathrm{AWI\text{-}O2}}$, $F_{\mathrm{s\text{-}O2}}$, and $F_{\mathrm{w\text{-}O2}}$) do not change significantly during this period (pseudo steady state), Eq. S23 becomes

$$\bar{C}_{\mathrm{w-O2}} - \bar{C}^{\mathrm{sat}}_{\mathrm{w-O2}} = (\frac{F_{\mathrm{AWI-O2}}}{H} + \frac{F_{\mathrm{s-O2}}}{H} + \frac{F_{\mathrm{w-O2}}}{H})T \quad \text{Eq. S24}$$

Where $\bar{C}^{\mathrm{sat}}_{\mathrm{w-O2}}$ is the average saturation oxygen concentration in the water column at in-situ temperatures. Thus, the LHS of Eq. S24 equals the negative average water column apparent oxygen utilization (AOU):

$$(\bar{C}_{\mathrm{w-O2}} - \bar{C}^{\mathrm{sat}}_{\mathrm{w-O2}}) = (\int_0^H -\mathrm{AOU}\,\mathrm{d}z_w)/H = -\overline{\mathrm{AOU}} \quad \text{Eq. S25}$$

Eqs. S24, S25 and S22 can then be combined:

$$-\overline{\mathrm{AOU}} \times H = F_{\mathrm{AWI-O2}} T + T\left(1 + \frac{1}{\varepsilon}(e^{fH} - 1)\right) F_{\mathrm{s-O2}} \quad \text{Eq. S26}$$

and

$$\overline{\mathrm{AOU}} \times H = F_{\mathrm{AWI-O2}} T + T\left(1 + \frac{1}{\varepsilon}(e^{fH} - 1)\right) \mathrm{SOU} \quad \text{Eq. S27}$$

S2.5 Oxygen mass balance in the bottom boundary layer (BBL)

Similar to the oxygen mass balance in the whole water column (Eq. S6), the changes in O_2 concentrations in the BBL is contributed by fluxes from the upper water column, sediments, and consumption within the BBL:

$$\frac{\mathrm{d}\bar{C}_{\mathrm{BBL-O2}}}{\mathrm{d}t} = \frac{F_{\mathrm{BI-O2}}}{h} + \frac{F_{\mathrm{s-O2}}}{h} + \frac{F_{\mathrm{BBL-O2}}}{h} \quad \text{Eq. S28}$$

Here, $\bar{C}_{\mathrm{BBL\text{-}O2}}$ is the integrated oxygen concentration in the BBL divided by the thickness the BBL (h): $\bar{C}_{\mathrm{BBL-O2}} = (\int_{H-h}^{h} C_{\mathrm{BBL-O2}}\,\mathrm{d}z_{\mathrm{w}})/h$, which is also the average O_2 concentration in the BBL. $F_{\mathrm{BI\text{-}O2}}$ is the flux of O_2 across the interface (boundary) between the BBL and the upper waters (positive means downward flux, and oxygen enters the BBL); $F_{\mathrm{BBL\text{-}O2}}$ is the oxygen reaction flux in the BBL, defined as the integrated O_2 rate in the BBL.

Similar to Eq. S15, by using the upper boundary of the BBL (z_{w}= H-h) as the reference, the concentration of organic matter in the BBL is

$$C_{\mathrm{w-C}} = C_{\mathrm{w-C}}^{H-h} e^{-k_{\mathrm{w}}\left(\frac{z_{\mathrm{w}}-(H-h)}{u_{\mathrm{w}}}\right)} = C_{\mathrm{w-C}}^{H-h} e^{-\left(\frac{k_{\mathrm{w}}}{u_{\mathrm{w}}}\right)(z_{\mathrm{w}}-(H-h))} \quad \text{Eq. S29}$$

where $C_{\mathrm{w-C}}^{H-h}$ is the concentration of organic carbon at depth H-h (the boundary of the upper boundary of the BBL). Organic carbon concentration at the SWI is

$$C_{\mathrm{w-C}}^{H} = C_{\mathrm{w-C}}^{H-h} e^{-\left(\frac{k_{\mathrm{w}}}{u_{\mathrm{w}}}\right)h} \quad \text{Eq. S30}$$

Therefore, by combining Eq. S13 and Eq. S30, the sediment oxygen flux becomes

$$F_{\mathrm{s-O2}} = -\varepsilon C_{\mathrm{w-C}}^{H} u_{\mathrm{w}} = -\varepsilon C_{\mathrm{w-C}}^{H-h} e^{-\left(\frac{k_{\mathrm{w}}}{u_{\mathrm{w}}}\right)h} u_{\mathrm{w}} \quad \text{Eq. S31}$$

Similar to Eq. S17, O_2 reaction flux in the BBL is defined as

$$F_{\mathrm{BBL-O2}} = \int_{H-h}^{H} -k_{\mathrm{w}} C_{\mathrm{w-C}}\,\mathrm{d}z_{\mathrm{w}} \quad \text{Eq. S32}$$

By combining Eqs. S32 and S29,

$$F_{\mathrm{BBL-O2}} = \int_{H-h}^{H} -k_{\mathrm{w}} C_{\mathrm{w-C}}^{H-h} e^{-\left(\frac{k_{\mathrm{w}}}{u_{\mathrm{w}}}\right)(z_{\mathrm{w}}-(H-h))}\,\mathrm{d}z_{\mathrm{w}} = C_{\mathrm{w-C}}^{H-h} u_{\mathrm{w}} (e^{-\left(\frac{k_{\mathrm{w}}}{u_{\mathrm{w}}}\right)h} - 1) \quad \text{Eq. S33}$$

Therefore, combining Eqs. S33 and S31 we can get the relationship between the flux of oxygen in the BBL and the sediments:

$$F_{\mathrm{BBL-O2}} = \frac{1}{\varepsilon}\left(e^{\left(\frac{k_{\mathrm{w}}}{u_{\mathrm{w}}}\right)h} - 1\right) F_{\mathrm{s-O2}} = \frac{1}{\varepsilon}\left(e^{fh} - 1\right) F_{\mathrm{s-O2}} \quad \text{Eq. S34}$$

Similar to Eq. S26, we can obtain the O_2 budget for the BBL the loss of O_2 from saturation concentration to the current state over a period of T :

$$-\overline{\mathrm{AOU}}_{\mathrm{BBL}} \times h = F_{\mathrm{BI-O2}} T + T\left(1 + \frac{1}{\varepsilon}(e^{fh} - 1)\right) F_{\mathrm{s-O2}} \quad \text{Eq. S35}$$

and

$$\overline{\mathrm{AOU}}_{\mathrm{BBL}} \times h = F_{\mathrm{BI-O2}} T + T\left(1 + \frac{1}{\varepsilon}(e^{fh} - 1)\right) \mathrm{SOU} \quad \text{Eq. S36}$$

In **summary**, the oxygen mass balance in the whole water column can be simplified as:

$$\overline{\mathrm{AOU}} \times H = F_{\mathrm{AWI-O2}} T + T\left(1 + \frac{1}{\varepsilon}(e^{fH} - 1)\right)\mathrm{SOU} \qquad \text{Eq. S27}$$

The oxygen mass balance in the bottom boundary layer can be simplified as:

$$\overline{\mathrm{AOU}}_{\mathrm{BBL}} \times h = F_{\mathrm{BI-O2}} T + T\left(1 + \frac{1}{\varepsilon}(e^{fh} - 1)\right)\mathrm{SOU} \qquad \text{Eq. S36}$$

Where T is the time needed to develop the current AOU; ε is the efficiency of organic matter remineralization in sediments; f is the spatial frequency of organic matter remineralization in the water column.

S3. Spatial reactivity (*f*) of organic matter in the water column

The spatial reactivity ($f = k_w/u_w$) describes the reaction proceeded per-unit distance the particles settle downwards. By fitting the observation ($F_{s\text{-}O2}$, h, H, and AOU calculated) to the model (Eqs. S27 and S36) using a sediment recycling efficiency of ε= 0.5 and a reaction time (also time for stratification to sustain) of T = 15 d, we obtain an organic matter spatial reactivity of f = 0.026 m^{-1} for the PRE region. During our sampling period, there was a typhoon that had potentially disrupts the water column stratification. Therefore, the water column CTD data obtained right after the typhoon were excluded when fitting the model. A comparison of observation and model is shown in Figure S7.

We can check the order of magnitude of f using a separate estimation of the rate of organic matter remineralization in the water column. For an organic matter production rate of 66 mmol m^{-2} d^{-1} in the region (Cai et al., 2004) and an average SOU of 41.1±16.3 mmol m^{-2} d^{-1}, about 28% of the organic matter remineralization occurs in the water column (100%- 41.1/66*100% = 28%). Therefore, from Eq. S21,

$$f = \frac{-\mathrm{d}C_{\mathrm{w-C}}}{C_{\mathrm{w-C}}\,\mathrm{d}z_w} \qquad \text{Eq. S37}$$

For water column total depth (H = dz_w) of 10-20 m, the spatial reactivity is f=0.28/H = 0.014-0.028 m^{-1}. This is an order of magnitude consistent with the model fitting results.

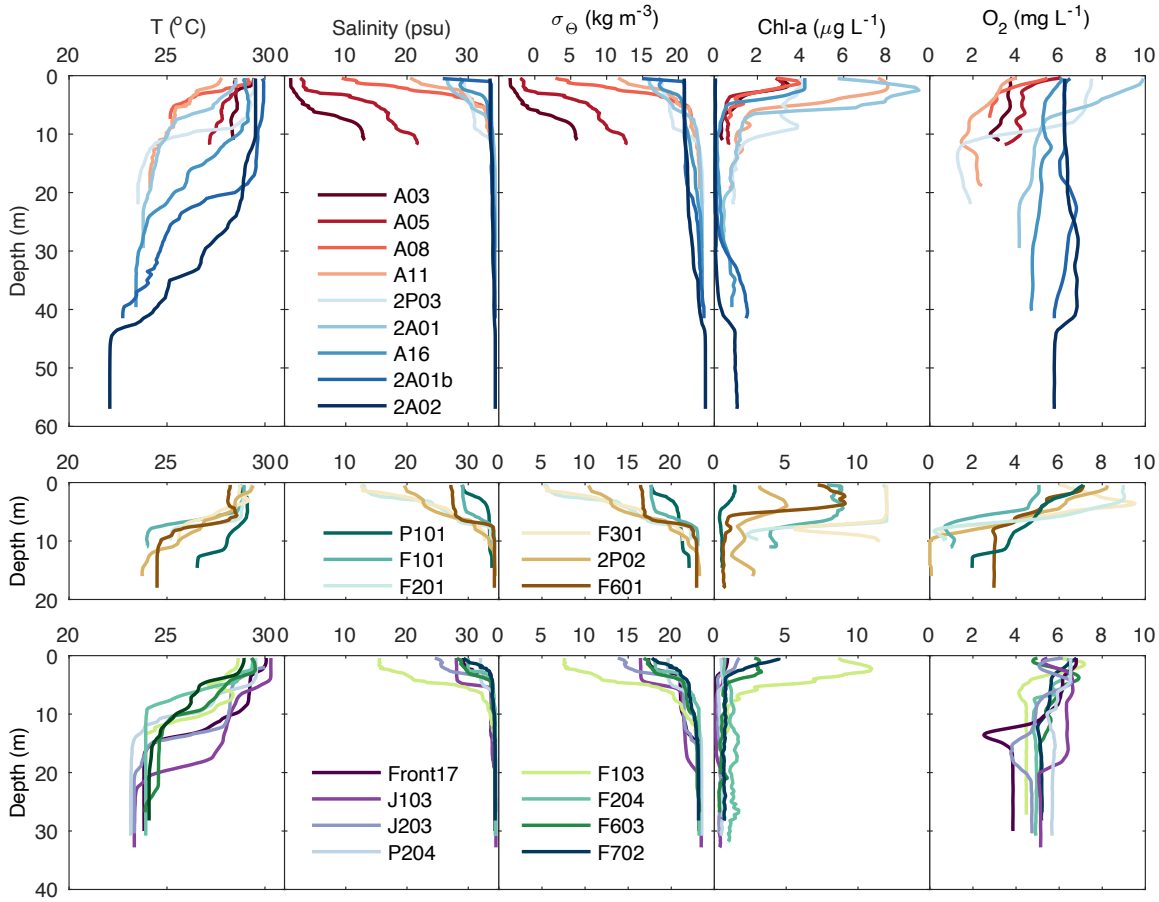

Figure S1 Vertical distributions of temperature, salinity, sigma density (σ_Θ), chlorophyl a (chl-a), and oxygen concentrations in the water column.

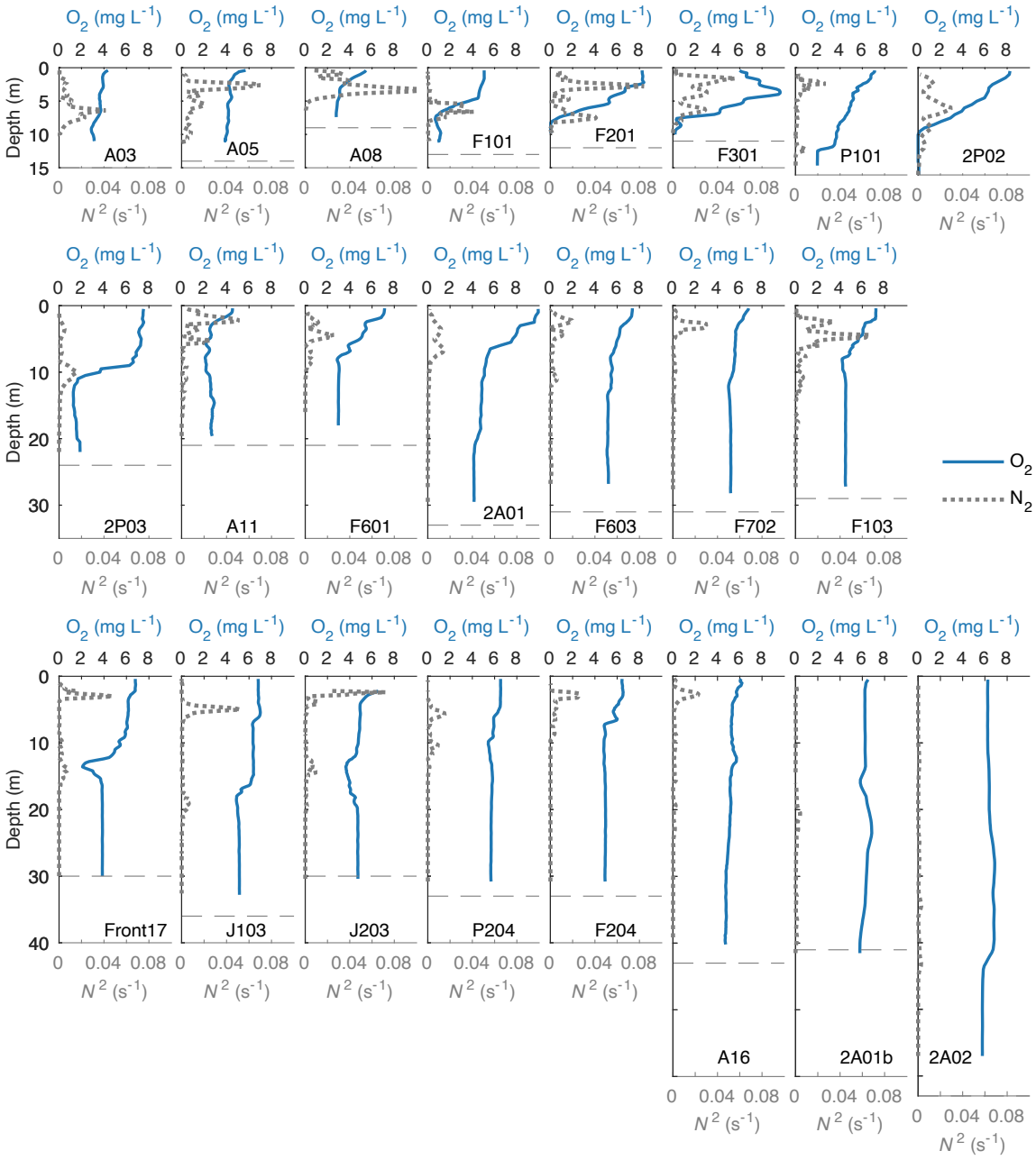

Figure S2 Vertical distributions of buoyance frequency (N^2) and oxygen concentrations in the water column. Horizontal dash lines represent the seafloor.

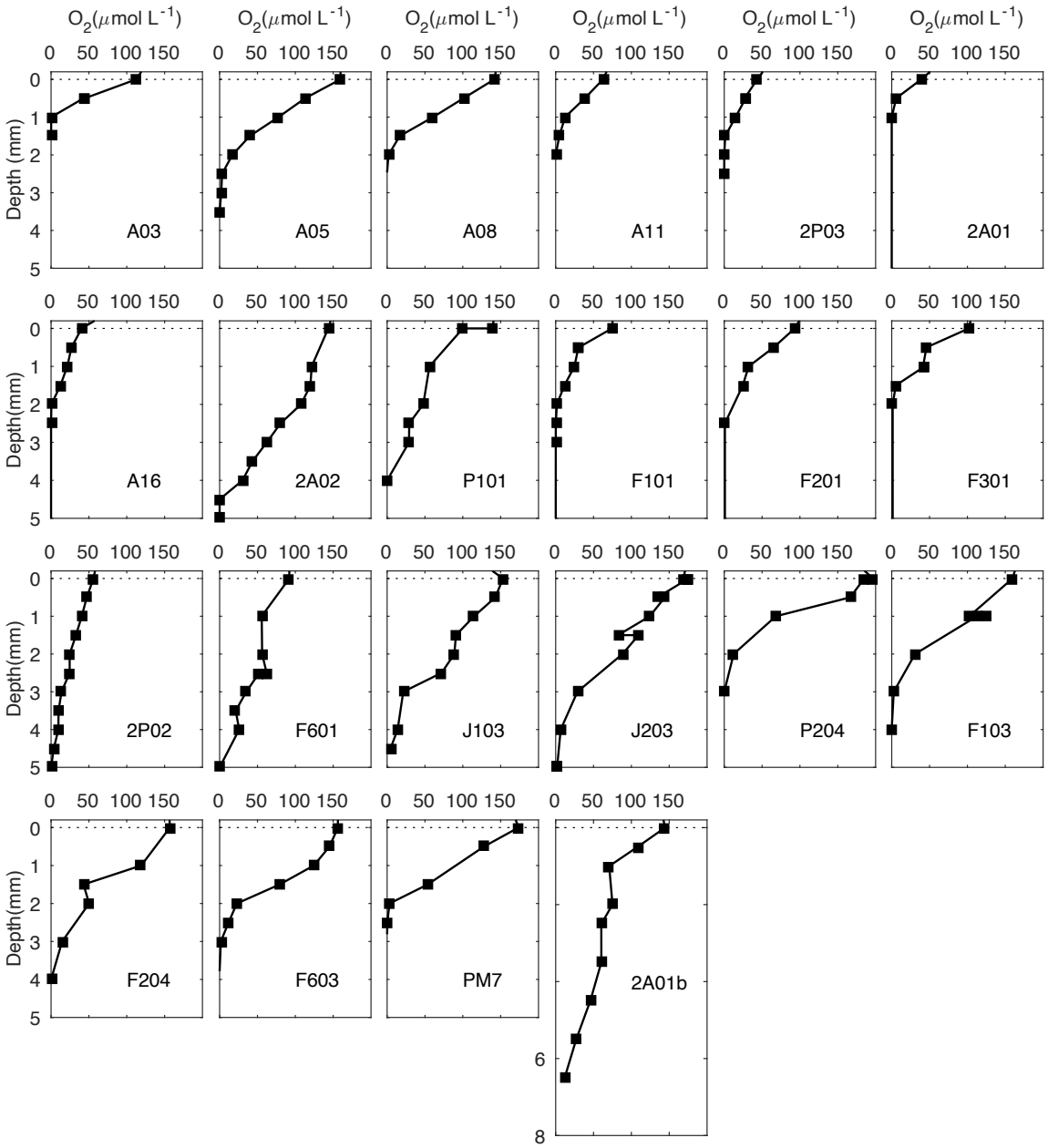

Figure S3 Oxygen profiles in the sediments.

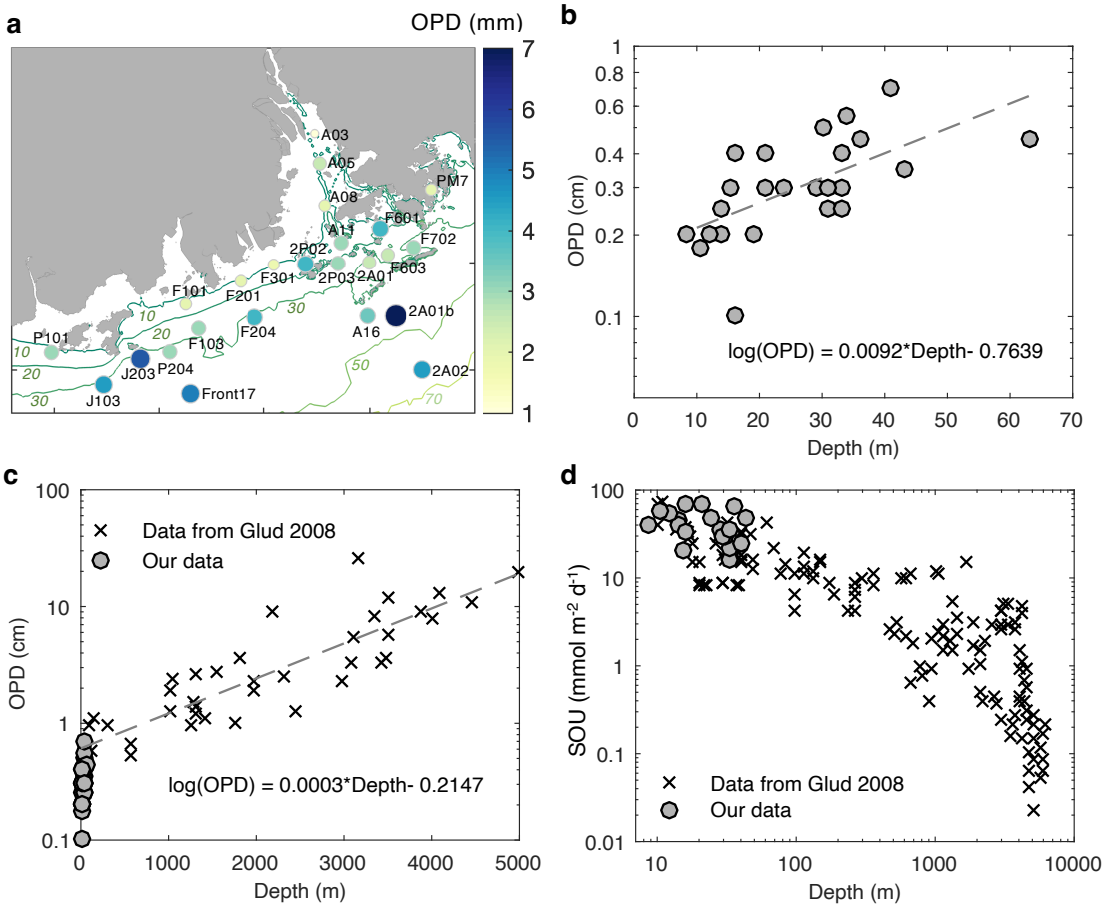

Figure S4 a) Spatial distribution of sediment oxygen penetration depth (OPD) in the Pearl River Estuary and adjacent shelf; **b**) OPD vs total water depth in the PRE region; **c**) OPD vs total water depth in the global ocean (Glud, 2008); **d**) Sediment oxygen uptake in the PRE region compared to that of global marine sediments (Glud, 2008).

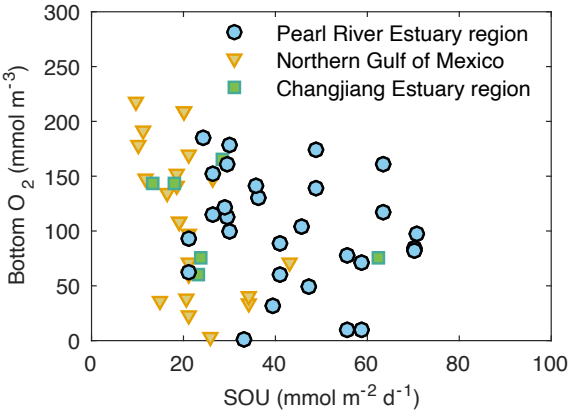

Figure S5 Bottom oxygen concentration vs sediment oxygen uptake from PRE region, northern Gulf of Mexico (McCarthy et al., 2013a), and the Changjiang Estuary region (Zhang et al., 2017).

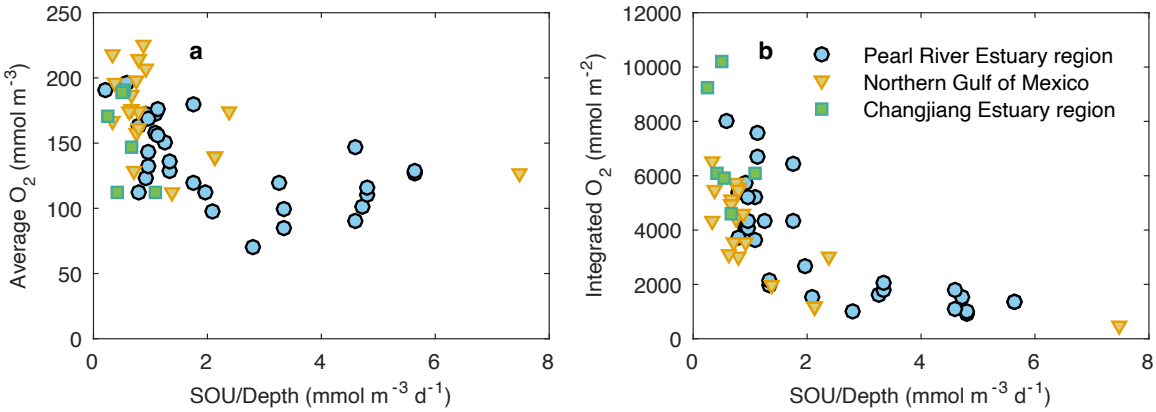

Figure S6 a) Average oxygen concentration and B) integrated O_2 concentrations in the whole water column vs SOU normalized to total water depth (SOU/Depth) in the Pearl River Estuary region, northern Gulf of Mexico (McCarthy et al., 2013a), and the Changjiang Estuary region (Zhang et al., 2017).

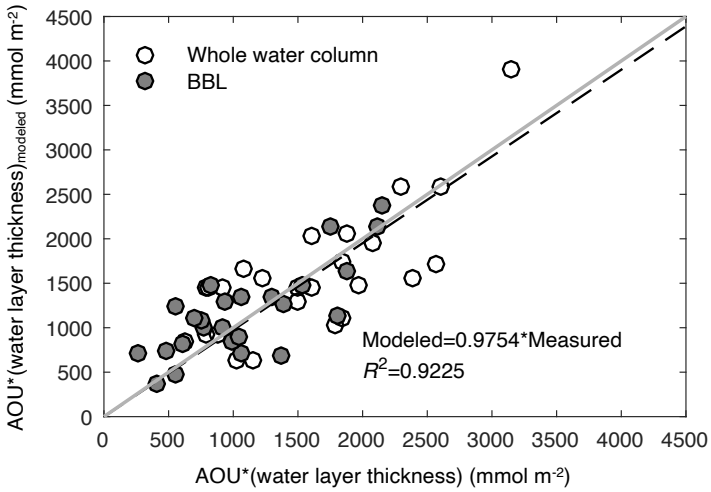

Figure S7 Model apparent oxygen utilizations (AOU) compared to measured AOU for the BBL and the whole water column.

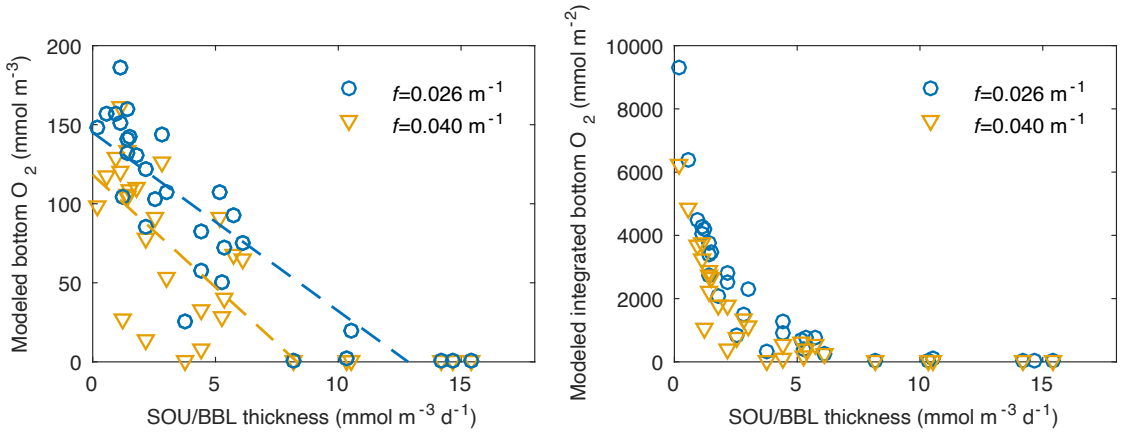

Figure S8 Modeled bottom O_2 level under different spatial reactivity of organic matter (*f*).

Table S1. Sampling locations, water depth, thickness of the BBL, bottom water O_2, oxygen penetration depth (OPD), sediment oxygen uptake (SOU), apparent oxygen utilization in the water column and BBL (AOU and AOU_{BBL}).

Date (mm/dd/yy)	Station	Latitude (°N)	Longitude (°E)	Depth (m)	BBL thickness (m)	Bottom O_2 (μmol L^{-1})	Average O_2 (μmol L^{-1})	AOU (mmol m^{-3})	AOU_{BBL} (mmol m^{-3})	OPD (mm)	SOU (mmol m^{-2} d^{-1})
04/09/2021*	PM7	114.211	22.340	19						2.0	
06/03/2021*	A03	113.741	22.602	15	6.8	97.3	102.0	125.5	120.1	1.0	70.5
06/03/2021*	A05	113.765	22.463	14	8.0	105.0	118.7	107.1	113.2	2.5	45.8
06/04/2021*	A08	113.788	22.266	9	3.9	87.9	110.6	103.8	122.9	2.0	41.0
06/21/2021		113.78	22.279	8	2.8	59.7	115.9	93.8	149.3		
06/04/2021*	A11	113.866	22.093	21	15.8	83.3	85.0	123.8	134.1	3.0	70.4
06/21/2021		113.866	22.095	21	15.9	82.5	99.7	109.7	127.2		
06/04/2021*	A16	113.99	21.752	43	39.9	139.3	155.6	54.7	50.7	3.5	49.0
06/22/2021		113.99	21.752	43	23.0	173.6	176.6	32.5	42.6		
06/05/2021*	P101	112.488	21.581	16	3.4	62.7	128.3	74.6	121.7	3.0	20.9
06/19/2021		112.581	21.584	15	8.2	92.2	136.3	66.6	109.7		
06/07/2021*	F103	113.189	21.694	29	21.3					3.0	35.9
06/19/2021		113.189	22.694	29	24.3	140.2	150.8	63.3	72.8		
06/07/2021*	F101	113.129	21.937	13	5.6					2.0	39.4
06/19/2021		113.128	21.806	15	7.6	31.6	70.0	130.9	168.4		
06/08/2021*	F201	113.389	21.914	12	3.9	9.1	147.1	65.4	199.9	2.0	55.4
06/20/2021		113.388	21.912	12	10.0	77.4	90.0	124.7	140.2		
06/15/2021*	F301	113.548	21.990	11	3.8	8.9	126.3	87.6	197.5	1.8	59.0
06/21/2021		113.547	21.991	10	7.2	70.5	128.4	76.3	88.6		
06/06/2021	J203	112.913	21.551	34	30.3	108.2	118.6	91.1	94.2		
06/17/2021*		112.919	21.551	34	19.7	147.8	144.1	63.8	77.5	5.5	
06/17/2021*	Front17	113.150	21.390	30	16.0	120.6	143.8	65.6	94.4	5.0	29.2
06/06/2021	J103	112.740	21.430	36	21.4	117.0	120.4	87.6	100.6		
06/18/2021*		112.738	21.431	36	29.8	160.3	179.1	31.6	34.1	4.5	63.5
06/06/2021	P204	113.052	21.592	33	20.9	100.0	123.0	77.8	93.4		
06/19/2021*		113.052	21.584	33	21.3	108.8	172.7	32.9	36.9	3.0	30.0
06/08/2021	F204	113.463	21.746	33	23.2	115.6	113.1	94.2	115.1		
06/20/2021*		113.456	21.744	33	28.6	153.1	163.9	48.4	54.4	4.0	26.3
06/11/2021	F603	114.084	22.038	31	10.5	113.1	132.5	77.2	100.3		
06/22/2021*		114.085	22.037	31	26.7	161.3	169.4	36.7	43.4	2.5	29.7
06/11/2021	F702	114.213	22.070	31	12.0	100.0	143.8				
06/22/2021*		114.124	22.412	31	26.5	156.3	168.8				
06/11/2021	F601	114.050	22.159	21	20.0	173.0	173.0	30.2	30.2		
06/22/2021*		114.050	22.159	21	14.7	93.8	124.7	85.6	105.3	4.0	
07/01/2021*	2A01	113.998	22.001	33	26.5	131.0	157.6	48.5	71.0	2.5	36.4
07/04/2021*	2A02	114.252	21.501	63	63	166.9	191.3	10.2	36.3	4.5	14.0
07/06/2021*	2P03	113.851	21.997	24	13.3	50.3	112.8	86.3	70.0	3.0	47.4
07/06/2021*	2P02	113.698	21.994	16	6.5	1.4	97.2	112.0	221.9	1.0	33.4
07/08/2021*	2A01b	114.123	21.751	41	41	184.5	196.4	8.6	13.6	7.0	24.4

Table S2 List parameters and variables

H	Total depth of the water column [m]
z_w	The vertical displacement in the water column with the sea surface as zero and positive going downward [m]
z_s	The vertical displacement in the sediment column with the sediment-water interface as zero and positive going downward [m].
$C_{w\text{-}O2}$	O_2 concentration in the water column [mmol m^{-3}]
$\bar{C}_{w-O2} = \left(\int_0^H C_{w-O2}\, dz_w\right)/H$	Average O_2 concentration in the water column [mmol m^{-3}], defined as $C_{w\text{-}O2}$ integrated along the entire water column divided by the total depth H.
$\bar{C}^{sat}_{w-O2} = \left(\int_0^H C^{sat}_{w-O2}\, dz_w\right)/H$	Average saturation O_2 concentration in the water column at in-situ temperature [mmol m^{-3}], defined as the saturation O_2 concentration $C_{w\text{-}O2}$ integrated along the entire water column divided by the total depth H.
$C_{s\text{-}O2}$	O_2 concentration in the sediment [mmol m^{-3}]
$R_{w\text{-}O2}$	Reaction rate of O_2 in the water column [mmol m^{-3} d^{-1}]
$R_{s\text{-}O2}$	Reaction rate of O_2 in sediments [mmol m^{-3} d^{-1}]
$F_{AWI\text{-}O2}$	O_2 fluxes at the air-water interface [mmol m^{-2} d^{-1}]
$F_{SWI\text{-}O2}$	O_2 fluxes at the sediment-water interface [mmol m^{-2} d^{-1}], positive downwards, also defined as sediment oxygen uptake (SOU)
$F_{w\text{-}O2}=\int_0^H R_{w-O2}\, dz_w$	O_2 reaction flux in the water column [mmol m^{-2} d^{-1}], defined as the integration of the O_2 rate ($R_{w\text{-}O2}$) over the entire water column
$F_{s\text{-}O2}=\int_0^{+\infty} R_{s-O2}\, dz_s$	O_2 reaction flux in the sediment [mmol m^{-2} d^{-1}], defined as the integration of the O_2 rate ($R_{s\text{-}O2}$) over the entire sediment column
$C_{s\text{-}C}$	Organic carbon concentration in the sediment [mmol m^{-3}]
$C^0_{s\text{-}C}$	Organic carbon concentration in the sediments at the sediment-water interface (z_s=0) [mmol m^{-3}]
$C_{w\text{-}C}$	Organic carbon concentration in the water column [mmol m^{-3}]
$C^0_{w\text{-}C}$	Organic carbon concentration in the surface water (z_w=0) [mmol m^{-3}]
$C^H_{w\text{-}C}$	Organic carbon concentration in the sediments at the sediment-water interface (z_w=H) [mmol m^{-3}]
k_s	Reactivity of organic carbon in sediments [d^{-1}]
k_w	Reactivity of organic carbon in the water column [d^{-1}]
u_s	Burial velocity of sediments [m d^{-1}]
u_w	Settling velocity of particles in the water column [m d^{-1}]
$f = k_w/u_w$	Spatial frequency [m^{-1}], defined as the temporal frequency (rates k_w) divided by the settling velocity u_w.
t	Time (d)
ε	The efficiency of organic carbon remineralization in sediments
T	The time needed for the water column to reach the current level of oxygen from an oxygen-saturated condition.
AOU=$C^{sat}_{w-O2} - C_{w-O2}$	Apparent oxygen utilization in the water column [mmol m^{-3}], defined as the difference between oxygen concentration at saturation and the measured oxygen concentration in the water.
$\overline{AOU} = \frac{\int_0^H (C^{sat}_{w-O2} - C_{w-O2})\, dz_w}{H} = \bar{C}^{sat}_{w-O2} - \bar{C}_{w-O2}$	Average AOU in the water column [mmol m^{-3}], defined as AOU integrated over the entire water column divided by the total depth H.
h	The thickness of the bottom boundary layer [m].
$\bar{C}_{BBL-O2} = \left(\int_{H-h}^H C_{w-O2}\, dz_w\right)/h$	Average O_2 concentration in BBL [mmol m^{-3}], defined as O2 concentration ($C_{w\text{-}O2}$) integrated over the BBL divided by the thickness of the BBL h.
$F_{BI\text{-}O2}$	The flux of O_2 across the interface (boundary) between the BBL and the upper waters (positive means downward flux, and oxygen enters the BBL) [mmol m^{-2} d^{-1}].
$F_{BBL-O2} = \int_{H-h}^H R_{w-O2}\, dz_w$	the oxygen reaction flux in the BBL, defined as the integrated O_2 rate in the BBL.
$-\overline{AOU}_{BBL} = \frac{\int_{H-h}^H (C^{sat}_{w-O2} - C_{w-O2})\, dz_w}{H} = \bar{C}^{sat}_{BBL-O2} - \bar{C}_{BBL-O2}$	Average AOU in the BBL [mmol m^{-3}], defined as AOU integrated over the BBL divided by the thickness of the layer h.

Table S3 Water column oxygen and sediment oxygen uptake from other coastal systems

Region	Site ID	Depth (m)	BBL*/hypoxia+/ pycnocline^ thickness (m)	Bot. O_2 (mg/L)	Aver. O_2 (mg/L)	SOU (mmol m^{-2} d^{-1})	Ref
Changjiang Estuary region	H18_Aug	58	35.7*	2.40	3.59	24.0	a
Changjiang Estuary region	H19_Jun	58	35.0*	4.60	5.48	13.5	a
Changjiang Estuary region	H9_Aug	34	15.9*	1.96	4.70	23.2	a
Changjiang Estuary region	H9_Jun	34	14.0*	4.57	6.08	18.2	a
Changjiang Estuary region	H15_Aug	57	29.0*	2.40	2.56	62.5	a
Changjiang Estuary region	H15_Jun	57	27.7*	5.30	6.03	28.6	a
Northern Gulf of Mexico	C6_Aug09	19	8.3*	0.10	3.62	26.1	b
Northern Gulf of Mexico	CT2_Aug09	28	14.6*	4.52	5.96	18.7	b
Northern Gulf of Mexico	F5_Aug09	29	9.7*	3.44	5.64	19.3	b
Northern Gulf of Mexico	F5_Aug09	29	16.9*	3.44	5.64	19.3	b
Northern Gulf of Mexico	MRM_Aug09	10	5.8*	3.09	4.49	21.3	b
Northern Gulf of Mexico	MRM_Aug09	10	1.9*	0.76	4.49	21.3	b
Northern Gulf of Mexico	MRM_Aug09	10	3.4*	2.30	4.49	21.3	b
Northern Gulf of Mexico	C6_May10	18	10.7*	2.27	5.60	43.2	b
Northern Gulf of Mexico	CT2_May10	28	8.5*	1.22	4.13	20.4	b
Northern Gulf of Mexico	F5_May10	29	9.0*	1.93	5.03	21.2	b
Northern Gulf of Mexico	MRM_May10	10	1.3*	1.11	4.09	34.3	b
Northern Gulf of Mexico	C6_May11	19	3.3*	1.15	5.15	15.0	b
Northern Gulf of Mexico	CT2_May11	33	28.0*	4.74	5.58	26.4	b
Northern Gulf of Mexico	F5_May11	29	12.7*	5.43	6.35	21.4	b
Northern Gulf of Mexico	C6_Sep08	19	19.0*	4.70	5.55	11.5	b
Northern Gulf of Mexico	CT2_Sep08	29	19.0*	5.69	5.33	9.9	b
Northern Gulf of Mexico	F5_Sep08	28	28.0*	6.10	6.28	11.0	b
Northern Gulf of Mexico	B7_Jan09	21	21.0*	4.86	7.24	18.5	b
Northern Gulf of Mexico	C6_Jan09	18	6.0*	4.31	6.62	16.5	b
Northern Gulf of Mexico	CT2_Jan09	25	18.7*	6.70	6.87	20.4	b
Northern Gulf of Mexico	CT2_Jan09	25	25.3*	6.70	6.87	20.4	b
Northern Gulf of Mexico	F5_Jan09	30	30.0*	6.98	6.70	9.8	b
Northern Gulf of Mexico	MRM_May11	10	2.5*	1.28	5.15	34.3	b
Middle Chesapeake Bay	CB3.2C	13	7.0^	0.80		61.4	c
Middle Chesapeake Bay	CB4.1C	32	11.5^	0.10		25.7	c
Middle Chesapeake Bay	CB4.3C	27	12.4^	0.23		14.3	c
Middle Chesapeake Bay	CB5.1	28	16.5^	0.90		21.4	c
Middle Chesapeake Bay	CB5.2	30	15.1^	1.01		15.8	c
Gulf of St Lawrence			100+	< 2.0		9.7	d
Long Island Sound			12+	< 2.0		19	e
Northwestern Black Sea			9+	< 2.0		6.8	f
Baltic Sea			125+	< 2.0		8	g

Note:

a) Sediment oxygen uptake (SOU) are from Zhang et al., (2017) and the water column parameters are calculated from CTD profiles provided by the author H. Zhang.
b) SOU data are from McCarthy et al., (2013) and water column parameters are calculated from CTD profiles provide by the author M. J. McCarthy.
c) SOU data are from Boynton et al., (2022); water column data for the corresponding sites are from the Chesapeake Bay Program (CBP, https://datahub.chesapeakebay.net).
d) Fennel and Testa 2019 (originally from Lehmann et al., (2009))
e) Fennel and Testa 2019 (originally from Welsh & Eller, (1991))
f) Fennel and Testa 2019 (originally from Cannaby et al., (2015), Capet et al., (2013), and Capet et al., (2016))
g) Fennel and Testa 2019 (originally from Noffke et al., (2016) and Wulff & Stigebrandt (1989))

Reference

APHA (1998) Standard Methods for the Examination of Water and Wastewater. 20th Edition, American Public Health Association, American Water Works Association and Water Environmental Federation, Washington DC.

Boynton, W. R., Ceballos, M. A. C., Hodgkins, C. L. S., Liang, D., & Testa, J. M. (2022). Large-Scale Spatial and Temporal Patterns and Importance of Sediment–Water Oxygen and Nutrient Fluxes in the Chesapeake Bay Region. *Estuaries and Coasts*, 1–20. https://doi.org/10.1007/s12237-022-01127-0

Cai, W. J., Dai, M., Wang, Y., Zhai, W., Huang, T., Chen, S., et al. (2004). The biogeochemistry of inorganic carbon and nutrients in the Pearl River estuary and the adjacent Northern South China Sea. *Continental Shelf Research*, *24*(12), 1301–1319. https://doi.org/10.1016/j.csr.2004.04.005

Cannaby, H., Fach, B. A., Arkin, S. S., & Salihoglu, B. (2015). Climatic controls on biophysical interactions in the Black Sea under present day conditions and a potential future (A1B) climate scenario. *Journal of Marine Systems*, *141*, 149–166. https://doi.org/10.1016/j.jmarsys.2014.08.005

Capet, A., Beckers, J.-M., & Grégoire, M. (2013). Drivers, mechanisms and long-term variability of seasonal hypoxia on the Black Sea northwestern shelf – is there any recovery after eutrophication? *Biogeosciences*, *10*(6), 3943–3962. https://doi.org/10.5194/bg-10-3943-2013

Capet, Arthur, Meysman, F. J. R., Akoumianaki, I., Soetaert, K., & Grégoire, M. (2016). Integrating sediment biogeochemistry into 3D oceanic models: A study of benthic-pelagic coupling in the Black Sea. *Ocean Modelling*, *101*, 83–100. https://doi.org/10.1016/j.ocemod.2016.03.006

Fennel, K., & Testa, J. M. (2019). Biogeochemical Controls on Coastal Hypoxia. *Annual Review of Marine Science*. Retrieved from https://doi.org/10.1146/annurev-marine-010318-095138

Glud, R. N. (2008). Oxygen dynamics of marine sediments. *Marine Biology Research*, *4*(4), 243–289. https://doi.org/10.1080/17451000801888726

Jørgensen, B. B., & Revsbech, N. P. (1985). Diffusive boundary layers and the oxygen uptake of sediments and detritus1. *Limnology and Oceanography*, *30*(1), 111–122. https://doi.org/10.4319/lo.1985.30.1.0111

Lehmann, M. F., Barnett, B., Gélinas, Y., Gilbert, D., Maranger, R. J., Mucci, A., et al. (2009). Aerobic respiration and hypoxia in the Lower St. Lawrence Estuary: Stable isotope ratios of dissolved oxygen constrain oxygen sink partitioning. *Limnology and Oceanography*, *54*(6), 2157–2169. https://doi.org/10.4319/lo.2009.54.6.2157

Li, J., Crowe, S. A., Miklesh, D., Kistner, M., Canfield, D. E., & Katsev, S. (2012). Carbon mineralization and oxygen dynamics in sediments with deep oxygen penetration, Lake Superior. *Limnology and Oceanography*, *57*(6), 1634–1650. https://doi.org/10.4319/lo.2012.57.6.1634

McCarthy, M. J., Carini, S. A., Liu, Z., Ostrom, N. E., & Gardner, W. S. (2013a). Oxygen consumption in the water column and sediments of the northern Gulf of Mexico hypoxic zone. *Estuarine, Coastal and Shelf Science*, *123*, 46–53. https://doi.org/10.1016/j.ecss.2013.02.019

McCarthy, M. J., Carini, S. A., Liu, Z., Ostrom, N. E., & Gardner, W. S. (2013b). Oxygen consumption in the water column and sediments of the northern Gulf of Mexico

hypoxic zone. *Estuarine, Coastal and Shelf Science*, *123*, 46–53. https://doi.org/10.1016/j.ecss.2013.02.019

McDougall, T. J., & Barker, P. M. (2011). *Getting started with TEOS-10 and the Gibbs Seawater (GSW) Oceanographic Toolbox* (Vol. SCOR/IAPSO WG127). SCOR/IAPSO WG127.

Middelburg, J. J. (1989). A simple rate model for organic matter decomposition in marine sediments. *Geochimica et Cosmochimica Acta*, *53*(7), 1577–1581. https://doi.org/10.1016/0016-7037(89)90239-1

Noffke, A., Sommer, S., Dale, A. W., Hall, P. O. J., & Pfannkuche, O. (2016). Benthic nutrient fluxes in the Eastern Gotland Basin (Baltic Sea) with particular focus on microbial mat ecosystems. *Journal of Marine Systems*, *158*, 1–12. https://doi.org/10.1016/j.jmarsys.2016.01.007

Welsh, B. L., & Eller, F. C. (1991). Mechanisms controlling summertime oxygen depletion in western Long Island Sound. *Estuaries*, *14*(3), 265–278. https://doi.org/10.2307/1351661

Wulff, F., & Stigebrandt, A. (1989). A time-dependent budget model for nutrients in the Baltic Sea. *Global Biogeochemical Cycles*, *3*(1), 63–78. https://doi.org/10.1029/gb003i001p00063

Zhang, H., Zhao, L., Sun, Y., Wang, J., & Wei, H. (2017). Contribution of sediment oxygen demand to hypoxia development off the Changjiang Estuary. *Estuarine, Coastal and Shelf Science*, *192*, 149–157. https://doi.org/10.1016/j.ecss.2017.05.006

Zhou, L. (2022). *Sediment oxygen uptake and carbon mineralization in the Pearl River Estuary and adjacent coastal waters*. Master's Thesis, The Hong Kong University of Science and Technology. doi: 10.14711/thesis-991013088359403412.